ACS NANO
Cite This: ACS Nano 2018, 12, 6545−6553
www.acsnano.org

ARTICLE

Designing Optoelectronic Properties by On-Surface Synthesis: Formation and Electronic Structure of an Iron−Terpyridine Macromolecular Complex

Agustin Schiffrin,[†,§,⊥,∞] Martina Capsoni,[†,∞] Gelareh Farahi,[†] Chen-Guang Wang,[¶] Cornelius Krull,[§] Marina Castelli,[§] Tanya Roussy,[†] Katherine A. Cochrane,[∥] Yuefeng Yin,[§,⊥,#] Nikhil V. Medhekar,[⊥,#] Michael Fuhrer,[§,⊥] Adam Q. Shaw,[†] Wei Ji,[*,¶] and Sarah A. Burke[*,†,‡,∥]

[†]Department of Physics and Astronomy, University of British Columbia, Vancouver, British Columbia, Canada, V6T 1Z1
[‡]Quantum Matter Institute, University of British Columbia, Vancouver, British Columbia, Canada, V6T 1Z4
[§]School of Physics & Astronomy, Monash University, Clayton, Victoria 3800, Australia
[⊥]ARC Centre of Excellence in Future Low-Energy Electronics Technologies, Monash University, Clayton, Victoria 3800, Australia
[∥]Department of Chemistry, University of British Columbia, Vancouver, British Columbia, Canada, V6T 1Z1
[¶]Department of Physics and Beijing Key Laboratory of Optoelectronic Functional Materials & Micro-nano Devices, Renmin University of China, Beijing 100872, People's Republic of China
[#]Department of Materials Science and Engineering, Monash University, Clayton, Victoria 3800, Australia

Supporting Information

ABSTRACT: **Supramolecular chemistry protocols applied on surfaces offer compelling avenues for atomic-scale control over organic−inorganic interface structures. In this approach, adsorbate−surface interactions and two-dimensional confinement can lead to morphologies and properties that differ dramatically from those achieved *via* conventional synthetic approaches. Here, we describe the bottom-up, on-surface synthesis of one-dimensional coordination nanostructures based on an iron (Fe)-terpyridine (tpy) interaction borrowed from functional metal−organic complexes used in photovoltaic and catalytic applications. Thermally activated diffusion of sequentially deposited ligands and metal atoms and intraligand conformational changes lead to Fe−tpy coordination and formation of these nanochains. We used low-temperature scanning tunneling microscopy and density functional theory to elucidate the atomic-scale morphology of the system, suggesting a linear tri-Fe linkage between facing, coplanar tpy groups. Scanning tunneling spectroscopy reveals the highest occupied orbitals, with dominant contributions from states located at the Fe node, and ligand states that mostly contribute to the lowest unoccupied orbitals. This electronic structure yields potential for hosting photoinduced metal-to-ligand charge transfer in the visible/near-infrared. The formation of this unusual tpy/tri-Fe/tpy coordination motif has not been observed for wet chemistry synthetic methods and is mediated by the bottom-up on-surface approach used here, offering pathways to engineer the optoelectronic properties and reactivity of metal−organic nanostructures.**

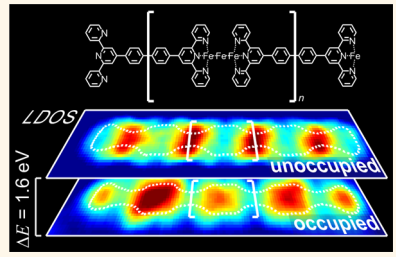

KEYWORDS: *self-assembly, scanning tunneling microscopy, scanning tunneling spectroscopy, coordination polymers, low-dimensional nanostructures, surface chemistry, density functional theory*

A crucial challenge for (opto)electronics technologies relying on organic molecules and polymers remains control over solid-state structure, particularly at interfaces.[1,2] Bottom-up supramolecular self-assembly techniques offer exquisite control over nanoscale structure and properties, allowing for the synthesis of mesoscopic structures from carefully designed molecular tectons, with atomic-scale precision and without external intervention.[3] When applied on a surface, these approaches have yielded a wide range of low-dimensional supramolecular systems with high fidelity,[4,5] yet few have demonstrated the emergence of deliberately sought physicochemical functionalities.[6−8] The robust bonding[9,10] and

Received: February 7, 2018
Accepted: May 30, 2018
Published: June 18, 2018

DOI: 10.1021/acsnano.8b01026
ACS Nano 2018, 12, 6545−6553

vast range of physical and chemical properties found in coordination complexes, tuned *via* choice of the metal center and ligand environment, offer a promising avenue for engineering both structure and functionality *via* self-assembly.[11−13] In particular, polypyridyl-based metal−organic complexes and coordination polymers exhibit an extensive range of optoelectronic, spin, and chemical properties that can be exploited in technological applications, such as photovoltaics,[14] catalysis,[15,16] molecular electronics,[17,18] molecular magnetism,[19] and biomedicine.[20,21] Complexes consisting of group 8 transition metals—iron, ruthenium, and osmium—coordinated with bis- and terpyridine (tpy) ligands have received special attention due to their photophysical properties, including optical transitions (from the ultraviolet to near-infrared) related to intramolecular photoinduced metal-to-ligand charge transfer (MLCT). These properties can give rise to efficient photoinduced charge separation needed for photovoltaics[22,23] and photocatalysis.[24] The robustness and well-defined morphology of the metal−polypyridyl coordination motif further allows for the design of hierarchical metallo-supramolecular structures[25−27] with a similarly rich array of physical properties, while offering additional avenues of control over the structure and environment by tuning both intra- and intermolecular interactions through ligand modification.[28,29]

Extending the functional motif of these coordination complexes to surface-bound protocols of supramolecular chemistry[4,30,31] offers practical advantages in terms of both synthesis and nanoscale control for device design, *e.g.*, in photovoltaics and heterogeneous catalysis, where active materials are in contact with a solid substrate. However, the surface introduces both challenges and opportunities to the robust design of bottom-up nanostructures: interactions with the substrate may alter the intended intrinsic properties, potentially allowing for the formation of structures with coordination symmetries, metal oxidation states, and polyatomic metal centers[9,32,33] that are markedly different from those achieved *via* wet-chemistry-based synthetic methods [*i.e.*, where precursors are not confined to two dimensions (2D)]. Such distinct structures will also manifest distinct electronic properties through changes in the underlying electronic states.

Here, we describe the formation, morphology, and electronic structure of linear self-assembled metal−organic nanostructures *via* thermally activated coordination of bis-terpyridine (bis-tpy)-based ligands (terpyridine-phenyl−phenyl-terpyridine; TPPT) with iron (Fe) adatoms on a Ag(111) surface. These surface-supported macromolecular complexes were synthesized through sequential and independent deposition of the ligand and of the transition metal, providing a flexible methodology to tune the electronic properties of the resulting structures. Scanning tunneling microscopy (STM) and spectroscopy (STS) performed in ultrahigh vacuum (UHV) at low temperature, together with density functional theory (DFT), were used to determine the atomic-scale morphology and electronic states of the metal−organic chains. Our STM data, supported by DFT calculations, hint toward an unusual trinuclear Fe coordination linkage between coplanar tpy groups of facing quasi-flat TPPT ligands, enabled by the bottom-up on-surface synthetic approach, very different from related wet-chemistry-synthesized macromolecular complexes. Notably, our STS measurements reveal an electronic structure indicative of an MLCT absorption band, reminiscent of optical excitations in the visible/near-infrared (vis/NIR) of $Fe(tpy)_2$ complexes in solution.[34,35] These surface-bound macromolecular structures offer opportunities for controlling optoelectronic and catalytic function.

RESULTS

Figure 1a shows an STM image of TPPT molecules on Ag(111), before the deposition of Fe (see Methods). The molecule—imaged as a "dog bone"—adsorbs on the surface with a planar geometry, similar to other tpy-containing molecules.[36] Details on the nanoscale adsorption morphology and electronic structure of TPPT on Ag(111) can be found

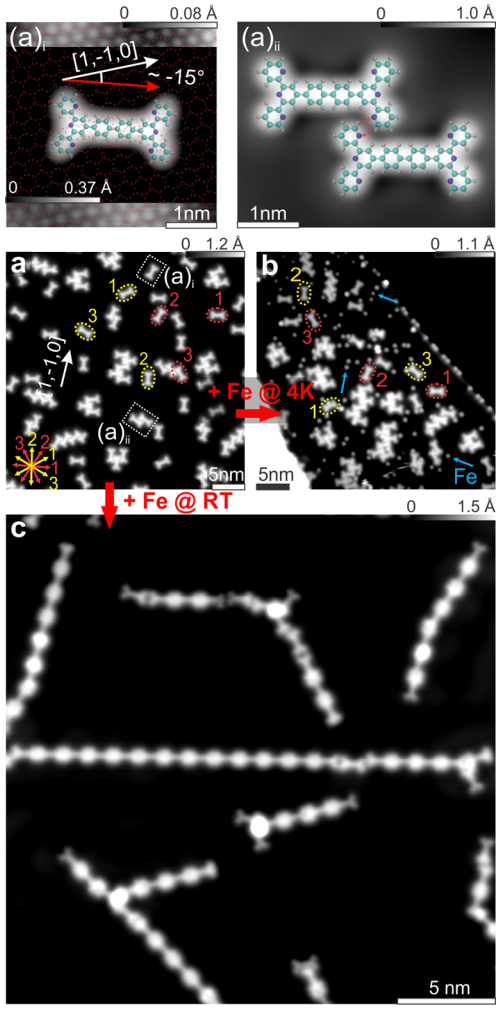

Figure 1. Low-temperature STM imaging of metal−organic nanochain formation. (a) Terpyridine-phenyl−phenyl-terpyridine (TPPT) molecule deposited on Ag(111) at room temperature (V_b = 200 mV, I_t = 50 pA). Molecules adsorb at a ~±15° (red and yellow dashed ellipses) angle with respect to the ⟨1, 1, 0⟩ crystallographic directions (white arrow), resulting in six energetically equivalent orientations (labels 1, 2, and 3). $(a)_i$ High-resolution images of a single TPPT molecule [similar to dashed box $(a)_i$ in panel (a); molecule: V_b = −200 mV, I_t = 10 pA; Ag(111): V_b = −10 mV, I_t = 300 nA] and $(a)_{ii}$ of a TPPT dimer formed *via* hydrogen bonds between peripheral pyridine groups [similar to dashed box $(a)_{ii}$ in (a); V_b = −100 mV, I_t = 50 pA]. Blue: nitrogen, cyan: carbon; white: hydrogen. (b) Fe adatoms (solid turquoise arrows) deposited on TPPT/Ag(111) at ~4.3 K (V_b = 500 mV, I_t = 10 pA). (c) Fe deposited at room temperature on TPPT/Ag(111) (V_b = 20 mV, I_t = 25 pA), inducing the formation of metal−organic chains. Fe adatoms are incorporated into the linear nanostructures. Brighter round features correspond to Fe clusters.

DOI: 10.1021/acsnano.8b01026
ACS Nano 2018, 12, 6545−6553

elsewhere.[37] The molecules can bind to each other laterally, *via* attractive noncovalent interactions between peripheral pyridine (pyr) groups, forming staggered rows or zigzag patterns[37] (Figure 1a).

Figure 1b shows an STM topograph after Fe deposition onto the TPPT/Ag(111) system held at 4.3 K (see Methods). The Fe adatoms (bright protrusions marked with solid turquoise arrows in Figure 1b) are scattered randomly on the surface and do not perturb the TPPT motifs observed prior to their addition (Figure 1a). After annealing at 373 K the Fe/TPPT/Ag(111) system prepared at 4.3 K, or following Fe deposition onto TPPT/Ag(111) at room temperature (RT) (Figure 1c), the atomic and molecular species rearrange into linear nanostructures. In these nanochains, TPPTs no longer bind laterally to each other, as in Figure 1a, but in a head-to-head configuration. Some of the Fe atoms also bind to step edges and aggregate into clusters[38] (brighter round features in Figure 1c). At 4.3 K, transition metal adatoms[39,40] and nitrogen-containing aromatic molecules[41,42] are immobile and do not diffuse on close-packed noble metal surfaces. At RT and above, both molecules and metal adatoms can diffuse, with diffusion rates that at RT are at least an order of magnitude larger for group 8 transition metal atoms[39,40] than for conjugated organic molecules;[41] thermal activation is necessary to enable mobility of both components. An increase in average chain length can be achieved by annealing at higher temperature [*e.g.*, 373 K; see Supporting Information (SI)] or by increasing the annealing time (*e.g.*, ∼several minutes at RT). This increase is accompanied by a decrease in the number of isolated metalated molecules (*i.e.*, not incorporated in chains and with one or two tpy sites coordinated with Fe). This indicates that isolated Fe-coordinated TPPT serve as building blocks for the self-assembly of the coordination complexes.

To understand the first step in forming Fe−TPPT chains, we investigated the configuration of isolated TPPT molecules after Fe deposition, in which one or both tpy groups have interacted with Fe adatoms. Figure 2b shows an STM image of an isolated TPPT molecule where the left-hand tpy is identical to that of an isolated TPPT before[37] Fe deposition (see Figure 1a). The right-hand tpy appears brighter, with a central protrusion. The latter was not observed prior to Fe deposition. This is the result of at least one Fe adatom that has interacted with the tpy group. Since all observed tpy groups of TPPT show one of these two imaging characteristics, we conclude that the termination consists of either zero or one Fe atom, but not more, as this would appear distinct in STM imaging. This is confirmed by DFT simulations (see Figure 2e and Methods).

Closer examination of the negative bias STM images reveals small apparent depressions in the substrate (turquoise arrows in Figure 2b and c) adjacent to the outer pyr rings. These depressions, indicative of a lowered electronic density of the Ag substrate, can be explained by repulsion of the surface conduction electrons by the outward-pointing distal pyr groups. Conversely, the absence of these depressions for Fe-coordinated tpy groups (green arrows in Figure 2b,d) indicates a rotation of the distal pyridines toward the metal adatom, allowing them to fully participate in the metal−ligand coordination, again consistent with the DFT results (Figure 2e).

The molecular configuration with all three pyr rings of a metalated tpy group oriented with the N atoms toward the Fe has two implications for the adsorption geometries. The coordination with Fe, involving all three pyr's (which previously

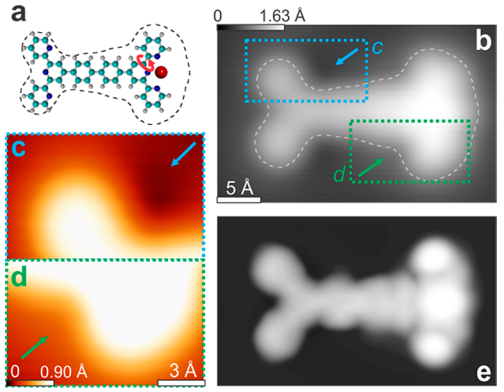

Figure 2. (a) Chemical structure (red: iron) and (b) STM image of a single TPPT with right tpy group coordinated to one Fe adatom (V_b = −200 mV, I_t = 1 nA). Coordination mediated by the rotation [red arrow in (a)] of peripheral pyr groups, which in the case of nonmetalated tpy [left tpy in (a)] point toward the outside of the molecule. Black dashed curve in (a) indicates molecular contour on the STM image in (b). (c, d) Zoomed-in details of regions *c* and *d* of STM image in panel (b). Nonmetalated tpy shows a depression (turquoise arrow) next to the peripheral pyr, not observed (green arrow) for metalated tpy (d). (e) DFT-simulated STM image (V_b = −200 mV) of a TPPT molecule with right tpy group coordinated to one Fe adatom, according to the structure in (a).

interacted significantly with the substrate), reduces the interaction of the molecule with the surface. This is consistent with the observed loss of preferential orientation of the Fe−TPPT chains with respect to the crystalline axes of the substrate (Figure 1c). Also, the zigzag and staggered intermolecular configurations, observed for pristine ligands[37] (Figure 1a) and characterized by lateral noncovalent interlocking between outward-pointing tpy groups of adjacent molecules, were not seen for tpy groups coordinated with Fe. Hence, thermal annealing of the Fe/TPPT system activates a configuration change of the tpy, enabling Fe−tpy coordination and altering intermolecular and molecule−substrate interactions.

Bias-dependent STM imaging and normalized $(dI/dV)/(I/V)$ STS[43] provide further insight into the morphology and electronic properties of the metalated molecule (Figure 3). Figure 3a shows an occupied-state STM image of a single TPPT, where each tpy group is coordinated with a single Fe atom (lateral positions indicated by vertical dashed turquoise lines), for a sample bias voltage of −0.5 V. Here, each tpy group is imaged identically to the right metalated tpy in Figure 2b, with a significant contribution to the imaging from the center of the tpy, where the Fe atom is located. Figure 3b shows an unoccupied-state STM image of the same metalated molecule, at +0.1 V. At this positive bias, the metalated tpy groups are V-shaped, similar to the nonmetalated tpy (see left tpy in Figure 2b); the areas where the Fe atoms are located contribute negligibly to the imaging. This is a strong indication that occupied Fe electronic states near the Fermi level contribute significantly to the highest occupied molecular orbitals (HOMOs) of the system, whereas empty Fe states have negligible contributions to the lowest unoccupied levels (LUMOs). This is emphasized in Figure 3c, corresponding to the subtraction of these images; bright regions indicate areas that contribute more to the HOMOs than to the LUMOs, with a clear bright protrusion at the center of the tpy group, where the Fe atom is located.

DOI: 10.1021/acsnano.8b01026
ACS Nano 2018, 12, 6545−6553

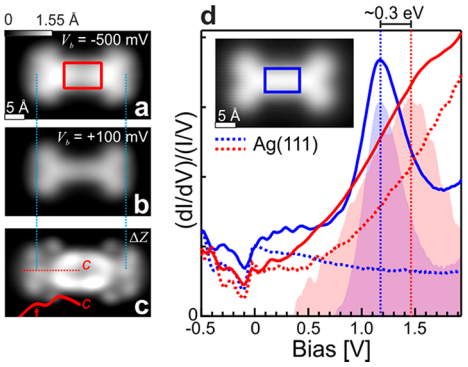

Figure 3. (a) Negative (−500 mV) and (b) positive (+100 mV) bias STM images of a single TPPT molecule with both tpy groups metalated with Fe adatoms (I_t = 200 pA). (c) Difference STM topographic map resulting from subtraction of (a) and (b). Vertical dashed turquoise lines indicate the lateral positions of single Fe adatoms coordinated with tpy. Solid red curve: Height profile along red dashed line *c*. Red arrow indicates a protrusion related to the Fe adatom. (d) Average $(dI/dV)/(I/V)$ spectra at the center of a single nonmetalated (blue) and Fe-coordinated (at both tpy groups; red) TPPT molecule. Dashed curves: Spectra on bare Ag(111) for pristine TPPT (blue) and Fe−TPPT (red) sample preparations. Blue and red spectra were acquired with tips with slightly different atomic-scale morphology and electronic signature, resulting in different reference bare Ag(111) spectra. Background filled curves (rescaled and offset for clarity): Difference spectra resulting from the subtraction of solid curves from dashed curves, to emphasize tunneling resonances [for both pristine (blue) and metalated (red) TPPT]. Within the bias voltage window considered, we did not observe clear tunneling resonances associated with occupied ligand states, and the spectra at large absolute values of negative bias (*e.g.*, V_b < −0.3 V; see SI) are dominated by tip features. Inset: STM image of a single, nonmetalated TPPT (V_b = −2.5 V, I_t = 50 pA). Rectangles indicate areas where spectra were taken.

Figure 3d displays $(dI/dV)/(I/V)$ spectra taken at the center of the single pristine (blue curve in Figure 3d) and doubly metalated (red) TPPT. The latter shows a clear tunneling resonance at ∼+1.5 V, given by contributions of ligand-related unoccupied states to the density of states (DOS). Notably, this feature is ∼+0.3 V above the tunneling resonance observed for pristine TPPT,[37] revealing a substantial change of the electronic properties of the molecule due to the metalation.

We now focus on structural details of the metal−organic nanochains. Similar to Figure 3, Figure 4a,b show high-resolution STM images of a chain composed of five TPPT molecules at different biases. The chains have a periodicity of 2.3 ± 0.2 nm. At a bias voltage of −0.5 V, STM imaging shows taller features at the Fe coordination centers. At +0.1 V, these regions are imaged as slight depressions compared to the surrounding ligand. As for the metalated TPPT in Figure 3, this indicates a significant contribution of the Fe electronic states to the occupied DOS in this region, whereas their contribution to the unoccupied DOS is limited. This is emphasized in the subtraction of these two topographic maps (Figure 4c). At each coordination center, we observe two clear protrusions separated by a distance of 5 ± 1 Å, which we can fit by two Gaussian curves (white dashed profiles in Figure 4c).

In order to better understand the structure of these chains, we modeled Fe−TPPT chains by DFT (see Methods) using periodic boundary conditions along the [1, −1, 0] axis of Ag(111) and a spacing of at least 8.7 Å between two neighboring chains along the [1, 1, −2] direction. Coordination linkages consisting of one, two, or three Fe adatoms were considered. The structure with three linearly arranged Fe atoms between the flat-lying tpy groups of the TPPT ligands (Figure 4d,h,i) was found to be most energetically favorable by 0.57 eV, with a periodicity of 2.32 nm, in excellent agreement with the experiment. A coordination configuration involving one or two adatoms is hindered by steric repulsion between the flat-lying tpy's. STM images simulated from the DFT model (Figure 4e,f; details in SI) reproduce the experimental data well (Figure 4a,b). Importantly, in the topographic map subtraction in Figure 4g, the 3-Fe coordination configuration appears as two bright protrusions separated by 4.2 ± 0.1 Å, given by the two tpy-bound Fe atoms (Fe_A and Fe_C in Figure 4h,i), being 0.74 Å higher than the central Fe (Fe_B), in good agreement with the experiment (Figure 4c). This agreement between simulated and

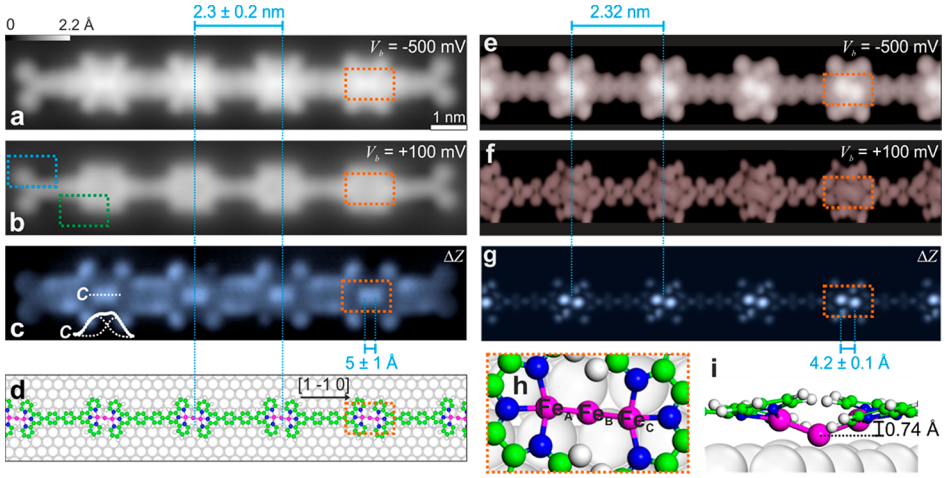

Figure 4. (a) Negative (−500 mV) and (b) positive (+100 mV) bias high-resolution STM images of a five-molecule Fe−TPPT nanochain (I_t = 1 nA). Turquoise (green) dashed box shows distal pyridine of a nonmetalated (metalated, respectively) tpy group (see Figure 2). (c) Difference STM topographic map resulting from subtraction of (a) and (b). Height profile *c* along the coordination center shows two protrusions fitted with Gaussians. (d) Model of the DFT-optimized metal−organic nanochain. (e) Negative and (f) positive bias DFT-simulated topographic STM images of the optimized Fe−TPPT/Ag(111) configuration. (g) DFT-simulated difference STM topographic map resulting from subtraction of (e) and (f). (h, i) Top and side view of the DFT-optimized coordination center.

DOI: 10.1021/acsnano.8b01026
ACS Nano 2018, 12, 6545−6553

experimental STM images supports the claim that the interligand binding is mediated by a tpy/tri-iron/tpy coordination scheme. See SI for further support for this linear tri-iron structure, ruling out other hypothetical structures. While similar trimetallic clusters have been observed for copper[33] (without the participation of the outer pyr's of the tpy group), this is a highly unusual and unexpected structure for Fe, mediated by the 2D confinement on the surface and facilitated by the UHV environment.

We explain the chain formation mechanism as follows. Upon deposition of atoms and molecules, thermal activation enables adsorbate diffusion and rotation of the TPPT distal pyr rings, allowing the tpy groups to coordinate with the Fe adatoms. The noble metal surface is crucial since it confines the system to 2D, enables efficient diffusion, and does not alter the molecular chemistry. Chain nucleation occurs when two metalated TPPT's *capture* and *lock* an additional Fe adatom. It is important to note that the observed metal−organic coordination cannot be explained by bridging residual gas ligands (*e.g.*, CO, H_2O) or adatoms from the Ag substrate (see SI).

We now turn to the electronic structure of this coordination complex. Figure 5a shows $dI/dV/(I/V)$ spectra[43] for the Fe center (orange) and the center of the TPPT ligand (red) in the metal−organic nanochain, compared with the pristine nonmetalated molecule (blue). Similarly to the double-metalated TPPT molecule in Figure 3, a ligand in a nanochain (see top-right STM topograph in Figure 5a) exhibits a clear tunneling resonance at a bias voltage of ∼+1.5 V, that is, ∼+0.3 V above the strong tunneling resonance associated with empty states located at the center of the pristine nonmetalated TPPT. A single TPPT molecule with both its tpy groups coordinated to a Fe adatom is thus (electronically) similar to a TPPT ligand within a metal−organic nanochain. Within the considered positive bias range (empty states), the differential conductance acquired on a Fe coordination center (orange curve in Figure 5a) does not show any clear tunneling resonance and is dominated by the exponential tunneling transmission function. However, a clear feature is observed for the Fe node at ∼−0.09 V. At this negative bias voltage, no feature was observed at the center of the pristine, nonmetalated TPPT[37] or at the center of the single Fe−TPPT−Fe in Figure 3d. This feature is emphasized by the background gray-filled curve in the inset of Figure 5a, corresponding to the ratio between the differential conductance at the Fe center and that at the ligand center. It is important to note that this negative bias $(dI/dV)/(I/V)$ feature associated with the Fe node was also clearly observed in non-normalized dI/dV spectra and local density of states spectra (retrieved according to Passoni *et al.*;[44] see Figure S4 in the SI); it is an intrinsic spectroscopic signature of occupied electronic states near the Fermi located at the Fe coordination node.

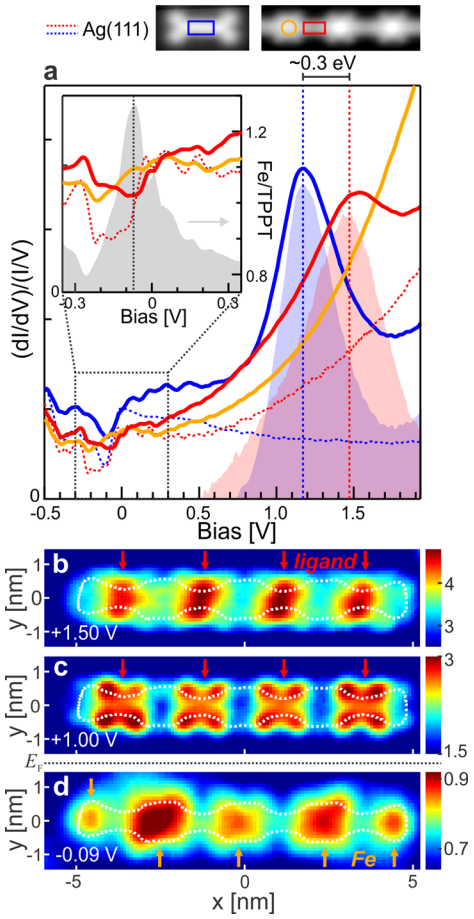

Figure 5. (a) Average $(dI/dV)/(I/V)$ spectra at the center of a single nonmetalated (blue) TPPT molecule (set point: V_b = −2.5 V, I_t = 50pA) of a ligand in an Fe−TPPT chain (red) and of an Fe coordination node (orange) (V_b = −2.5 V, I_t = 2.5 nA). Dashed curves: Spectra taken on bare Ag(111) for pristine TPPT (blue) and Fe−TPPT (red) sample preparations. Blue spectrum was acquired with a tip with atomic-scale morphology and electronic signature slightly different from that for red and orange spectra, resulting in different reference bare Ag(111) spectra. Above: STM images of a single nonmetalated TPPT molecule (left; V_b = −2.5 V, I_t = 50pA) and Fe−TPPT nanochain (right; V_b = −2.5 V, I_t = 2.5 nA). Rectangles and circle indicate areas where spectra were taken. Background filled curves (rescaled and offset for clarity): Difference spectra resulting from the subtraction of solid (blue, orange, red) curves with corresponding dashed curves. Inset: Detail of $(dI/dV)/(I/V)$ spectra near the Fermi level; background gray-filled curve corresponds to the ratio between spectra taken on the Fe node (orange) and ligand (red) in Fe-TPPT nanochain. (b−d) $(dI/dV)/(I/V)$ maps of a Fe−TPPT nanochain at V_b = −0.09, 1.00, and 1.50 V. Red (orange) arrows indicate positions of ligands (Fe coordination nodes) in (b) and (c) [(d), respectively].

DISCUSSION

Our STS data unequivocally show that the HOMOs of the metal−organic system have a dominant contribution from states located at the Fe coordination node (Figure 5d) and LUMOs with dominant contributions from ligand-related states (Figure 5b,c). These electronic properties are similar to those of complexes consisting of polypyridyl ligands coordinated in a octahedral geometry with a single Fe(II) atom, where Fe-dominated HOMOs and ligand-dominated LUMOs give rise to a visible light absorption band at photon energies $\hbar\omega$ > ∼2 eV (wavelengths λ < ∼600 nm).[23,34,35,45−47] Interestingly, the electronic properties of our quasi-flat, tri-iron complex are similar to these orthogonal, single Fe ones, despite the different coordination morphologies. In our case, the energy difference between the strong ligand-associated tunneling resonance at ∼1.5 eV (Figures 5a,b) and that related to the Fe node (∼−0.09 eV; Figure 5a,d) would potentially correspond to an optical transition in the vis/NIR (at $\hbar\omega$ < ∼1.59 eV, λ > ∼780 nm, given that the energy difference in the electronic tunneling spectrum in Figure 5a would typically be larger, by the exciton binding energy, than the energy involved in the associated photoexcitation). Here, the polarizability of the underlying noble metal substrate might arguably reduce this corresponding

DOI: 10.1021/acsnano.8b01026
ACS Nano 2018, 12, 6545−6553

electronic energy difference by screening the tunneling electrons and decreasing (increasing) the ionization potential (electron affinity, respectively); less polarizable substrates might result in larger electronic energy differences.

The likelihood of a potential optical transition associated with a photoinduced Fe-to-TPPT electron transfer would scale as $\propto|\varphi_i^*(\mathbf{r})(\nabla\varphi_f(\mathbf{r}))d\mathbf{r}|^2$, according to Fermi's golden rule,[48] with $\varphi_i(\mathbf{r})$ being the molecular orbital associated with the high $(dI/dV)/(I/V)$ at the Fe node (Figure 5d) and $\varphi_f(\mathbf{r})$ that at the ligand (Figure 5c,d). Here, the combination of spatial separation between the *centers of mass* of empty (Figure 5b,c) and occupied (Figure 5d) states, and at the same time significant spatial overlap between such states, can potentially give rise to efficient photoabsorption and photoinduced electron−hole separation in the vis/NIR, useful for photovoltaics and photocatalysis.

The positive energy shift (∼+0.3 eV) of the ligand-associated $(dI/dV)/(I/V)$ peak (∼+1.2 eV for the pristine TPPT; ∼+1.5 eV for TPPT in the chain; blue and red curves in Figure 5a) that accompanies the Fe−TPPT coordination can be explained by a decrease of the electron affinity (EA) of the molecule upon metal−ligand coordination. This decrease of EA is similar to that observed for an isolated, metalated TPPT that is not part of a chain (Figure 3d). This effect can be due to two phenomena: (i) reduction of interaction and electronic coupling between TPPT and Ag(111) upon Fe−tpy coordination, resulting in less screening of tunneling charge by the polarizable metal substrate [resulting in a $(dI/dV)/(I/V)$ peak energy resembling that of TPPT on an electronically decoupling NaCl layer on[37] Ag(111)]; (ii) Fe-to-TPPT electron transfer upon Fe−TPPT coordination. A coordination-induced reduction of the TPPT−surface electronic interaction would arguably result in a narrower, sharper $(dI/dV)/(I/V)$ peak [on NaCl, the full width at half-maximum (fwhm) of the $(dI/dV)/(I/V)$ peak related to the center[37] of TPPT is ∼0.2 eV]. This was not observed in our experiments (fwhm of background red-filled curve in Figure 5a is ∼0.65 eV). We can hence conclude that the observed decrease of ligand EA is most likely due to a coordination-induced metal-to-ligand electron transfer. This provides a further analogy and is consistent with the coordination-induced Fe-to-ligand electron transfer observed for single-Fe polypyridyl complexes with a octahedral coordination motif, where the Fe atom is in a +2 oxidation state.[46] A quantitative determination of the electronic configuration of each Fe atom in our metal−organic nanochains is beyond the scope of this study and requires further experimental and theoretical investigations.

The $(dI/dV)/(I/V)$ spectroscopic signature at ∼−0.09 eV associated with the Fe node (Figure 5a,d) lies at an energy slightly smaller than that of the Ag(111) Shockley surface state (SS) onset. This feature could be explained by a bound state located at the Fe node resulting from the coupling between an Fe energy level and the SS band.[49−51] However, a spectroscopic feature due to SS localization would differ substantially (see Figure S8 in the SI). In our case, the coplanar tpy's form a cavity that scatters the SS, minimizing the Fe−SS interaction and the likelihood of such coupling. Importantly, the spectroscopic signature of such SS-related bound state—which is claimed to be independent of the adsorbate[50]—was not observed for similar Cu-based metal−organic complexes on Cu(111) reported in a previous study.[33] In this previous study,[33] no HOMOs with dominant contributions from Cu adatom states were reported. We therefore ascribe our observed ∼−0.09 eV $(dI/dV)/(I/V)$ feature to electronic properties intrinsic to the Fe−tpy node.

CONCLUSIONS

In summary, we have shown the on-surface, bottom-up synthesis of metal−organic nanostructures based on the coordination of group 8 transition metal atoms with tpy compounds. The growth process is thermally driven and enabled by the on-surface approach, which provides 2D confinement and stabilizes the macromolecular complexes. Our experimental observations, supported by DFT, point to an unusual coordination motif consisting of a linear Fe trimer bonded to the coplanar tpy groups of the ligand and cannot be achieved *via* conventional wet-chemistry synthesis. The electronic structure of the system, including highest occupied (lowest unoccupied) states predominantly located at the transition metal center (ligand, respectively), is expected to give rise to photoinduced metal-to-ligand charge transfer in the vis/NIR, resulting in photophysical properties useful for photovoltaics and light-to-energy conversion technologies, in which atomic-scale structural control and interface engineering can lead to performance enhancement. Furthermore, the on-surface nanostructuring of well-defined group 8 transition metal clusters provides an interesting platform for site-isolated, heterogeneous catalysis with multimetallic centers. Applications might require translation of our approach to more functional substrates, other than the noble metal used in our model system here. For example, atomically flat 2D materials[52] (*e.g.*, graphene,[53] hexagonal boron nitride,[54] transition metal dichalcogenides[55]) offer balanced adsorbate−substrate interactions, similar to those on Ag(111), facilitating a similar self-assembly mechanism. Importantly, such 2D materials could provide electronic functionalities (semimetallic, insulating, semiconducting, respectively) useful for technological development and device implementation. Our approach offers pathways to investigate and tailor the optoelectronic properties and reactivity of metal−organic nanostructures from the bottom up.

METHODS

The metal−organic nanostructures were synthesized in UHV by sequential deposition of TPPT molecules (HetCat Switzerland) and Fe atoms from the gas phase onto a clean Ag(111) surface. The latter was prepared by repeated cycles of Ar^+ sputtering and annealing at 790 K. TPPT was sublimed at 550 K onto the Ag substrate held at RT, at a deposition rate of ∼4×10^{-4} molecules/(nm^2 s). The Fe atoms were subsequently evaporated onto the surface held at either 4.3 K (Figure 1b) or RT (Figure 1c). All STM and STS measurements were performed at 4.3 K with a Ag-terminated Pt/Ir tip. All topographic images were acquired in constant-current mode. STS measurements were obtained by measuring the tunneling current as a function of tip−sample bias voltage and tip position on the sample, with the tip height stabilized according to a constant-current set point at each location. The normalized numerical derivative[43] $dI/dV/(I/V)$ curves were computed as an approximation of the local density of states. The sample bias voltage is reported throughout the text. The base pressure was below 2×10^{-9} mbar during molecular deposition and below 1×10^{-10} mbar during Fe evaporation and STM and STS measurements.

DFT calculations were carried out within the generalized gradient approximation for the exchange correlation potentials, using the projector augmented waves method,[56,57] and a plane-wave basis set as implemented in the Vienna Ab-initio Simulation Package (VASP).[58,59] van der Waals interactions were included at the DFT-D2 level using the second version of Grimme's dispersion corrections[60] combined with the revised Perdew−Burke−Ernzerhof functional[61] (RPBE-G06),

DOI: 10.1021/acsnano.8b01026
ACS Nano 2018, 12, 6545−6553

which has been demonstrated to accurately describe molecule−metal interfaces.[62] A Tersoff−Hamman approximation was used within VASP to simulate STM images[63]

ASSOCIATED CONTENT

Supporting Information

The Supporting Information is available free of charge on the ACS Publications website at DOI: 10.1021/acsnano.8b01026.

DFT methods; DFT-simulated STM image of a singly Fe-metalated TPPT molecule; DFT-calculated distances between Fe atoms in the TPPT−Fe_3−TPPT complex; supporting evidence for the 3-Fe linkage structure; supplementary dI/dV STS data; bias-dependent STM data of single pristine and doubly metalated TPPT; dI/dV spectroscopic signature of isolated Fe and Fe in a nanochain; statistics of chain lengths at different growth temperatures (PDF)

AUTHOR INFORMATION

Corresponding Authors

*E-mail: wji@ruc.edu.cn. Phone: +86-10-62515597 (theory).
*E-mail: saburke@phas.ubc.ca. Phone: +1 (604)-822-8796 (experiments).

ORCID

Agustin Schiffrin: 0000-0003-1140-8485
Nikhil V. Medhekar: 0000-0003-3124-4430
Wei Ji: 0000-0001-5249-6624
Sarah A. Burke: 0000-0002-7337-0569

Author Contributions

∞A. Schiffrin and M. Capsoni contributed equally.

Notes

The authors declare no competing financial interest.

ACKNOWLEDGMENTS

S.A.B., M.C., A.S., T.R., G.F., K.C., and A.Q.S. acknowledge support from the Natural Sciences and Engineering Research Council (Discovery grants program No. 402072-2012), Canadian Foundation for Innovation (218484), British Columbia Knowledge Development Fund, Max Planck-UBC Centre for Quantum Materials (A.S.), Stewart Blusson Quantum Matter Institute (G.F.), Canada Research Chairs Program (S.B.), ARC Centre of Excellence for Future Low-Energy Electronics Technologies (A.S.), ACS Petroleum Research Fund (55955-ND5; M.C., S.A.B.), and University of British Columbia. W.J. and C.-G.W. were supported by the National Natural Science Foundation of China (Grant Nos. 11274380, 91433103, 11622437 and 61674171), the Fundamental Research Funds for the Central Universities, China and the Research Funds of Renmin University of China (Grant No. 16XNLQ01). The calculations were performed at the Physics Laboratory for High-Performance Computing of Renmin University of China and at the Shanghai Supercomputer Center. M.F. acknowledges support from the ARC Laureate Fellowship Programme. Y.Y. and N.V.M. acknowledge funding support from ARC Centre of Excellence for Future Low-Energy Electronics Technologies and computational support from the National Computing Infrastructure and Pawsey Supercomputing Facility.

REFERENCES

(1) Guo, X. G.; Zhou, N. J.; Lou, S. J.; Smith, J.; Tice, D. B.; Hennek, J. W.; Ortiz, R. P.; Navarrete, J. T. L.; Li, S. Y.; Strzalka, J.; Chen, L. X.; Chang, R. P. H.; Facchetti, A.; Marks, T. J. Polymer Solar Cells with Enhanced Fill Factors. *Nat. Photonics* **2013**, *7*, 825−833.

(2) Liu, Y. H.; Zhao, J. B.; Li, Z. K.; Mu, C.; Ma, W.; Hu, H. W.; Jiang, K.; Lin, H. R.; Ade, H.; Yan, H. Aggregation and Morphology Control Enables Multiple Cases of High-Efficiency Polymer Solar Cells. *Nat. Commun.* **2014**, *5* DOI: 10.1038/ncomms6293.

(3) Lehn, J. M. Supramolecular Chemistry: From Molecular Information Towards Self-Organization and Complex Matter. *Rep. Prog. Phys.* **2004**, *67*, 249−265.

(4) Barth, J. V. Molecular Architectonic on Metal Surfaces. *Annu. Rev. Phys. Chem.* **2007**, *58*, 375−407.

(5) Lin, N.; Stepanow, S.; Ruben, M.; Barth, J. V. Surface-Confined Supramolecular Coordination Chemistry. *Top. Curr. Chem.* **2008**, *287*, 1−44.

(6) Heim, D.; Ecija, D.; Seutert, K.; Auwarter, W.; Aurisicchio, C.; Fabbro, C.; Bonifazi, D.; Barth, J. V. Self-Assembly of Flexible One-Dimensional Coordination Polymers on Metal Surfaces. *J. Am. Chem. Soc.* **2010**, *132*, 6783−6790.

(7) Cai, J. M.; Pignedoli, C. A.; Talirz, L.; Ruffieux, P.; Sode, H.; Liang, L. B.; Meunier, V.; Berger, R.; Li, R. J.; Feng, X. L.; Mullen, K.; Fasel, R. Graphene Nanoribbon Heterojunctions. *Nat. Nanotechnol.* **2014**, *9*, 896−900.

(8) Bartels, L. Tailoring Molecular Layers at Metal Surfaces. *Nat. Chem.* **2010**, *2*, 87−95.

(9) Stepanow, S.; Lin, N.; Payer, D.; Schlickum, U.; Klappenberger, F.; Zoppellaro, G.; Ruben, M.; Brune, H.; Barth, J. V.; Kern, K. Surface-Assisted Assembly of 2D Metal-Organic Networks that Exhibit Unusual Threefold Coordination Symmetry. *Angew. Chem., Int. Ed.* **2007**, *46*, 710−713.

(10) Sun, Q.; Cai, L. L.; Ma, H. H.; Yuan, C. X.; Xu, W. On-Surface Construction of a Metal-Organic Sierpinski Triangle. *Chem. Commun.* **2015**, *51*, 14164−14166.

(11) Barth, J. V. Fresh Perspectives for Surface Coordination Chemistry. *Surf. Sci.* **2009**, *603*, 1533−1541.

(12) Friese, V. A.; Kurth, D. G. From Coordination Complexes to Coordination Polymers Through Self-Assembly. *Curr. Opin. Colloid Interface Sci.* **2009**, *14*, 81−93.

(13) Dong, L.; Gao, Z. A.; Lin, N. Self-Assembly of Metal-Organic Coordination Structures on Surfaces. *Prog. Surf. Sci.* **2016**, *91*, 101−135.

(14) Hardin, B. E.; Snaith, H. J.; McGehee, M. D. The Renaissance of Dye-Sensitized Solar Cells. *Nat. Photonics* **2012**, *6*, 162−169.

(15) Winter, A.; Newkome, G. R.; Schubert, U. S. Catalytic Applications of Terpyridines and Their Transition Metal Complexes. *ChemCatChem* **2011**, *3*, 1384−1406.

(16) Prier, C. K.; Rankic, D. A.; MacMillan, D. W. C. Visible Light Photoredox Catalysis with Transition Metal Complexes: Applications in Organic Synthesis. *Chem. Rev.* **2013**, *113*, 5322−5363.

(17) Tuccitto, N.; Ferri, V.; Cavazzini, M.; Quici, S.; Zhavnerko, G.; Licciardello, A.; Rampi, M. A. Highly Conductive ∼ 40-Nm-Long Molecular Wires Assembled by Stepwise Incorporation of Metal Centres. *Nat. Mater.* **2009**, *8*, 41−46.

(18) Sakamoto, R.; Katagiri, S.; Maeda, H.; Nishihara, H. Bis(Terpyridine) Metal Complex Wires: Excellent Long-Range Electron Transfer Ability and Controllable Intrawire Redox Conduction on Silicon Electrode. *Coord. Chem. Rev.* **2013**, *257*, 1493−1506.

(19) Real, J. A.; Gaspar, A. B.; Munoz, M. C. Thermal, Pressure and Light Switchable Spin-Crossover Materials. *Dalton Trans.* **2005**, 2062−2079.

(20) Gill, M. R.; Thomas, J. A. Ruthenium(II) Polypyridyl Complexes and DNA-from Structural Probes to Cellular Imaging and Therapeutics. *Chem. Soc. Rev.* **2012**, *41*, 3179−3192.

(21) Winter, A.; Gottschaldt, M.; Newkome, G. R.; Schubert, U. S. Terpyridines and Their Complexes with First Row Transition Metal

DOI: 10.1021/acsnano.8b01026
ACS Nano 2018, 12, 6545−6553

Ions: Cytotoxicity, Nuclease Activity and Self-Assembly of Biomacromolecules. *Curr. Top. Med. Chem.* **2012**, *12*, 158−175.
(22) Sauvage, J. P.; Collin, J. P.; Chambron, J. C.; Guillerez, S.; Coudret, C.; Balzani, V.; Barigelletti, F.; Decola, L.; Flamigni, L. Ruthenium(II) and Osmium(II) Bis(Terpyridine) Complexes in Covalently-Linked Multicomponent Systems - Synthesis, Electrochemical-Behavior, Absorption-Spectra, and Photochemical and Photophysical Properties. *Chem. Rev.* **1994**, *94*, 993−1019.
(23) Bowman, D. N.; Blew, J. H.; Tsuchiya, T.; Jakubikova, E. Elucidating Band-Selective Sensitization in Iron(II) Polypyridine-TiO_2 Assemblies. *Inorg. Chem.* **2013**, *52*, 8621−8628.
(24) Hurst, J. K. Water Oxidation Catalyzed by Dimeric μ-Oxo Bridged Ruthenium Diimine Complexes. *Coord. Chem. Rev.* **2005**, *249*, 313−328.
(25) Schubert, U. S.; Eschbaumer, C. Macromolecules Containing Bipyridine and Terpyridine Metal Complexes: Towards Metallosupramolecular Polymers. *Angew. Chem., Int. Ed.* **2002**, *41*, 2893−2926.
(26) Hofmeier, H.; Schubert, U. S. Recent Developments in the Supramolecular Chemistry of Terpyridine-Metal Complexes. *Chem. Soc. Rev.* **2004**, *33*, 373−399.
(27) Chiper, M.; Hoogenboom, R.; Schubert, U. S. Toward Main Chain Metallo-Terpyridyl Supramolecular Polymers: "The Metal Does the Trick". *Macromol. Rapid Commun.* **2009**, *30*, 565−578.
(28) Leong, W. L.; Vittal, J. J. One-Dimensional Coordination Polymers: Complexity and Diversity in Structures, Properties, and Applications. *Chem. Rev.* **2011**, *111*, 688−764.
(29) Furukawa, H.; Cordova, K. E.; O'Keeffe, M.; Yaghi, O. M. The Chemistry and Applications of Metal-Organic Frameworks. *Science* **2013**, *341*, 1230444.
(30) Stepanow, S.; Lin, N.; Barth, J. V. Modular Assembly of Low-Dimensional Coordination Architectures on Metal Surfaces. *J. Phys.: Condens. Matter* **2008**, *20*, 184002.
(31) Schlickum, U.; Decker, R.; Klappenberger, F.; Zoppellaro, G.; Klyatskaya, S.; Ruben, M.; Silanes, I.; Arnau, A.; Kern, K.; Brune, H.; Barth, J. V. Metal-Organic Honeycomb Nanomeshes with Tunable Cavity Size. *Nano Lett.* **2007**, *7*, 3813−3817.
(32) Stepanow, S.; Lingenfelder, M.; Dmitriev, A.; Spillmann, H.; Delvigne, E.; Lin, N.; Deng, X. B.; Cai, C. Z.; Barth, J. V.; Kern, K. Steering Molecular Organization and Host-Guest Interactions Using Two-Dimensional Nanoporous Coordination Systems. *Nat. Mater.* **2004**, *3*, 229−233.
(33) Wang, W. H.; Hong, Y. N.; Shi, X. Q.; Minot, C.; Van Hove, M. A.; Tang, B. Z.; Lin, N. Inspecting Metal-Coordination-Induced Perturbation of Molecular Ligand Orbitals at a Submolecular Resolution. *J. Phys. Chem. Lett.* **2010**, *1*, 2295−2298.
(34) Bernhard, S.; Goldsmith, J. I.; Takada, K.; Abruna, H. D. Iron(II) and Copper(II) Coordination Polymers: Electrochromic Materials with and without Chiroptical Properties. *Inorg. Chem.* **2003**, *42*, 4389−4393.
(35) Brown, A. M.; McCusker, C. E.; McCusker, J. K. Spectroelectrochemical Identification of Charge-Transfer Excited States in Transition Metal-Based Polypyridyl Complexes. *Dalton Trans.* **2014**, *43*, 17635−17646.
(36) Shi, X. Q.; Zhang, R. Q.; Minot, C.; Hermann, K.; Van Hove, M. A.; Wang, W. H.; Lin, N. Complex Molecules on a Flat Metal Surface: Large Distortions Induced by Chemisorption Can Make Physisorption Energetically More Favorable. *J. Phys. Chem. Lett.* **2010**, *1*, 2974−2979.
(37) Capsoni, M.; Schiffrin, A.; Cochrane, K. A.; Wang, C. G.; Roussy, T.; Shaw, A. Q.; Ji, W.; Burke, S. A. Selective Hybridization of a Terpyridine-Based Molecule with a Noble Metal. *J. Phys. Chem. C* **2017**, *121*, 23574−23581.
(38) Buchner, F.; Kellner, I.; Steinruck, H. P.; Marbach, H. Modification of the Growth of Iron on Ag(111) by Predeposited Organic Monolayers. *Z. Phys. Chem.* **2009**, *223*, 131−144.
(39) Knorr, N.; Brune, H.; Epple, M.; Hirstein, A.; Schneider, M. A.; Kern, K. Long-Range Adsorbate Interactions Mediated by a Two-Dimensional Electron Gas. *Phys. Rev. B: Condens. Matter Mater. Phys.* **2002**, *65*, 115420.
(40) Schiffrin, A.; Reichert, J.; Auwarter, W.; Jahnz, G.; Pennec, Y.; Weber-Bargioni, A.; Stepanyuk, V. S.; Niebergall, L.; Bruno, P.; Barth, J. V. Self-Aligning Atomic Strings in Surface-Supported Biomolecular Gratings. *Phys. Rev. B: Condens. Matter Mater. Phys.* **2008**, *78*, 035424.
(41) Eichberger, M.; Marschall, M.; Reichert, J.; Weber-Bargioni, A.; Auwarter, W.; Wang, R. L. C.; Kreuzer, H. J.; Pennec, Y.; Schiffrin, A.; Barth, J. V. Dimerization Boosts One-Dimensional Mobility of Conformationally Adapted Porphyrins on a Hexagonal Surface Atomic Lattice. *Nano Lett.* **2008**, *8*, 4608−4613.
(42) Kuhne, D.; Klappenberger, F.; Decker, R.; Schlickum, U.; Brune, H.; Klyatskaya, S.; Ruben, M.; Barth, J. V. Self-Assembly of Nanoporous Chiral Networks with Varying Symmetry from Sexiphenyl-Dicarbonitrile on Ag(111). *J. Phys. Chem. C* **2009**, *113*, 17851−17859.
(43) Zandvliet, H. J. W.; van Houselt, A. Scanning Tunneling Spectroscopy. *Annu. Rev. Anal. Chem.* **2009**, *2*, 37−55.
(44) Passoni, M.; Donati, F.; Bassi, A. L.; Casari, C. S.; Bottani, C. E. Recovery of Local Density of States Using Scanning Tunneling Spectroscopy. *Phys. Rev. B: Condens. Matter Mater. Phys.* **2009**, *79*, 045404.
(45) Liu, B.; Huang, H. X.; Zhang, C. F.; Chen, M.; Qian, D. J. Monolayers, Langmuir-Blodgett Films of Bimetallic Coordination Polymers of 4′-(4-Pyridyl)-2,2′:6′,2″-Terpyridine. *Thin Solid Films* **2008**, *516*, 2144−2150.
(46) Johnson, P. S.; Cook, P. L.; Zegkinoglou, I.; Garcia-Lastra, J. M.; Rubio, A.; Ruther, R. E.; Hamers, R. J.; Himpsel, F. J. Electronic Structure of Fe- vs. Ru-Based Dye Molecules. *J. Chem. Phys.* **2013**, *138*, 044709.
(47) Johansson, E. M. J.; Odelius, M.; Plogmaker, S.; Gorgoi, M.; Svensson, S.; Siegbahn, H.; Rensmo, H. Spin-Orbit Coupling and Metal-Ligand Interactions in Fe(II), Ru(II), and Os(II) Complexes. *J. Phys. Chem. C* **2010**, *114*, 10314−10322.
(48) Chen, C.; Bobisch, C. A.; Ho, W. Visualization of Fermi's Golden Rule through Imaging of Light Emission from Atomic Silver Chains. *Science* **2009**, *325*, 981−985.
(49) Olsson, F. E.; Persson, M.; Borisov, A. G.; Gauyacq, J. P.; Lagoute, J.; Folsch, S. Localization of the Cu(111) Surface State by Single Cu Adatoms. *Phys. Rev. Lett.* **2004**, *93*, 206803.
(50) Limot, L.; Pehlke, E.; Kroger, J.; Berndt, R. Surface-State Localization at Adatoms. *Phys. Rev. Lett.* **2005**, *94*, 036805.
(51) Lazarovits, B.; Szunyogh, L.; Weinberger, P. Spin-Polarized Surface States Close to Adatoms on Cu(111). *Phys. Rev. B: Condens. Matter Mater. Phys.* **2006**, *73*, 045430.
(52) Novoselov, K. S.; Mishchenko, A.; Carvalho, A.; Neto, A. H. C. 2D Materials and Van Der Waals Heterostructures. *Science* **2016**, *353*, aac9439.
(53) Jarvinen, P.; Hamalainen, S. K.; Banerjee, K.; Hakkinen, P.; Ijas, M.; Harju, A.; Liljeroth, P. Molecular Self-Assembly on Graphene on SiO_2 and H-Bn Substrates. *Nano Lett.* **2013**, *13*, 3199−3204.
(54) Urgel, J. I.; Schwarz, M.; Garnica, M.; Stassen, D.; Bonifazi, D.; Ecija, D.; Barth, J. V.; Auwarter, W. Controlling Coordination Reactions and Assembly on a Cu(111) Supported Boron Nitride Monolayer. *J. Am. Chem. Soc.* **2015**, *137*, 2420−2423.
(55) Kumar, A.; Banerjee, K.; Liljeroth, P. Molecular Assembly on Two-Dimensional Materials. *Nanotechnology* **2017**, *28*, 082001.
(56) Blochl, P. E. Projector Augmented-Wave Method. *Phys. Rev. B: Condens. Matter Mater. Phys.* **1994**, *50*, 17953−17979.
(57) Kresse, G.; Joubert, D. From Ultrasoft Pseudopotentials to the Projector Augmented-Wave Method. *Phys. Rev. B: Condens. Matter Mater. Phys.* **1999**, *59*, 1758−1775.
(58) Kresse, G.; Furthmuller, J. Efficient Iterative Schemes for *Ab Initio* Total-Energy Calculations Using a Plane-Wave Basis Set. *Phys. Rev. B: Condens. Matter Mater. Phys.* **1996**, *54*, 11169−11186.
(59) Kresse, G.; Furthmuller, J. Efficiency of *Ab-Initio* Total Energy Calculations for Metals and Semiconductors Using a Plane-Wave Basis Set. *Comput. Mater. Sci.* **1996**, *6*, 15−50.
(60) Grimme, S. Semiempirical GGA-Type Density Functional Constructed with a Long-Range Dispersion Correction. *J. Comput. Chem.* **2006**, *27*, 1787−1799.

DOI: 10.1021/acsnano.8b01026
ACS Nano 2018, 12, 6545−6553

(61) Hammer, B.; Hansen, L. B.; Norskov, J. K. Improved Adsorption Energetics within Density-Functional Theory Using Revised Perdew-Burke-Ernzerhof Functionals. *Phys. Rev. B: Condens. Matter Mater. Phys.* **1999**, *59*, 7413−7421.
(62) Hu, Z. X.; Lan, H. P.; Ji, W. Role of the Dispersion Force in Modeling the Interfacial Properties of Molecule-Metal Interfaces: Adsorption of Thiophene on Copper Surfaces. *Sci. Rep.* **2015**, *4*, 5036.
(63) Tersoff, J.; Hamann, D. R. Theory of the Scanning Tunneling Microscope. *Phys. Rev. B: Condens. Matter Mater. Phys.* **1985**, *31*, 805−813.

DOI: 10.1021/acsnano.8b01026
ACS Nano 2018, 12, 6545−6553